

# Journal of Materials Chemistry A

Accepted Manuscript



This is an *Accepted Manuscript*, which has been through the Royal Society of Chemistry peer review process and has been accepted for publication.

*Accepted Manuscripts* are published online shortly after acceptance, before technical editing, formatting and proof reading. Using this free service, authors can make their results available to the community, in citable form, before we publish the edited article. We will replace this *Accepted Manuscript* with the edited and formatted *Advance Article* as soon as it is available.

You can find more information about *Accepted Manuscripts* in the [Information for Authors](#).

Please note that technical editing may introduce minor changes to the text and/or graphics, which may alter content. The journal's standard [Terms & Conditions](#) and the [Ethical guidelines](#) still apply. In no event shall the Royal Society of Chemistry be held responsible for any errors or omissions in this *Accepted Manuscript* or any consequences arising from the use of any information it contains.



## Binary metal sulfide and polypyrrole on vertically-aligned carbon nanotubes array/carbon fiber paper as high-performance electrodes

Received 00th January 20xx,  
Accepted 00th January 20xx

DOI: 10.1039/x0xx00000x

www.rsc.org/

Xiaoyi Cai,<sup>a</sup> Reinack V. Hansen,<sup>c</sup> Lili Zhang,<sup>b</sup> Baosheng Li,<sup>d</sup> Chee Kok Poh,<sup>b</sup> San Hua Lim,<sup>b</sup> Luwei Chen,<sup>b</sup> Jinglei Yang,<sup>c</sup> Linfei Lai,<sup>a,\*</sup> Jianyi Lin,<sup>a</sup> Zexiang Shen<sup>a,\*</sup>

Pseudocapacitive materials, such as binary metal sulfides show great promise as electrode candidate for energy storage devices due to their higher specific capacitance than mono-metal sulfides and binary metal oxides, but generally suffer from low energy densities when assembled in supercapacitor devices. To push the energy density limit of pseudocapacitive materials in devices, a new class of electrode materials with favorable architectures is strongly needed. Here, a rational design and coaxial growth of Ni-Co-S and polypyrrole on vertically-aligned carbon nanotubes array (VA-CNTs)/3D carbon fiber paper (CFP) is presented as a novel freestanding electrode for energy storage devices. Our study has revealed that the catalyst preparation is the key step and the presence of the Al<sub>2</sub>O<sub>3</sub> buffer layer is essential to the growth of VA-CNTs. The 3D hierarchical VA-CNTs/CFP allows high areal loading and high utilization efficiency of the active materials. The binder-free asymmetric energy storage devices with Ni-Co-S/VA-CNTs/CFP as the positive electrode and polypyrrole/VA-CNTs/CFP as the negative electrode respectively demonstrates high energy density of 82 Wh/kg at 200 W/kg.

### Introduction

Carbon nanotubes (CNTs) are attractive nanomaterials with exceptional stiffness and strength, extraordinary thermal and electrical properties, high surface area and low density. Vertically aligned-carbon nanotubes (VA-CNTs) have certain advantages over bulk CNT powders and randomly oriented CNT mats due to their high degree of order and good controllability. However, CNTs synthesized by most of the common techniques, such as arc discharge and catalytic pyrolysis,[1] are often randomly entangled. The VA-CNTs are usually grown by chemical vapor deposition (CVD) on substrates with pre-deposited catalysts. Due to the rigorous CVD synthesis conditions, substrates used for the growth of VA-CNTs should be thermally and chemically stable, such as SiO<sub>2</sub>/Si wafers,[2] glasses,[3] MgO,[4] and Al<sub>2</sub>O<sub>3</sub> flake[5], most of which are 2D substrates with smooth surfaces. However, those substrates are insulating, and are not suitable

electrical conductivities.[6] Therefore, development of VA-CNTs on conductive, especially 3D hierarchical substrate remains both scientifically and technically challenging. Carbon fiber paper (CFP) is a 3D network consists of microsized carbon fibers with high porosity and good electric conductivity. 3D CFP has been studied extensively as substrates for fuel cell, batteries and supercapacitor electrodes. The growth of free standing VA-CNTs sheathed CFP with each individual carbon fiber coated uniformly with CNTs array provides a new class of multidimensional and multicomponent nanomaterials with well-defined surface and interfacial structures attractive for a wide range of potential applications.[7, 8]

Growing CNTs on carbon fiber surface was first reported by Thostenson et al.[9] CNTs sheathed carbon fibers by pyrolysis of FePc was developed by Qu et al., and pretreatment of carbon fibers with thin layer of SiO<sub>2</sub> by carbonizing SiCl<sub>4</sub> at 1000 °C in the presence of oxygen was required.[7] The same method was applied to the growth of CNT into thermally expanded HOPG interlayers.[10] The growth of VA-CNTs on CFP by an environmental friendly method (without using hazardous chemicals) will offer significant advantages and will be promising for various potential applications, including nanoelectronics, sensors, and energy storage devices.

Transition metal (hydr)oxides,[11, 12] sulfides,[13, 14] and conducting polymers[15, 16] are demonstrated as supercapacitor's electrodes based on their superior pseudocapacitive properties. More recently, metal sulfides have attracted extensive attention due to their high capacitance and excellent redox reversibility. High specific capacitance over 1000 F/g have been reported, such as NiCo<sub>2</sub>S<sub>4</sub> on Ni foam

<sup>a</sup> Energy Research Institute @ NTU (ERIAN), 1 CleanTech Loop, #06-04, CleanTech One, Singapore 637141. E-mail: [LALIF@ntu.edu.sg](mailto:LALIF@ntu.edu.sg); [Zexiang@ntu.edu.sg](mailto:Zexiang@ntu.edu.sg)

<sup>b</sup> Institute of Chemical and Engineering Sciences, A\*STAR, 1 Pesek Road, Jurong Island, 627833

<sup>c</sup> School of Mechanical & Aerospace Engineering, Nanyang Technological University, 50 Nanyang Avenue, Singapore 639798

<sup>d</sup> Key Laboratory of Flexible Electronics (KLOFE) & Institute of Advanced Materials (IAM), Jiangsu National Synergistic Innovation Center for Advanced Materials (SICAM), Nanjing Tech University (Nanjing Tech), 30 South Puzhu Road, Nanjing 211816, P. R. China

\*Electronic Supplementary Information (ESI) available: SEM images, CV curves. See DOI: 10.1039/x0xx00000x

for energy storage devices which require desirable integrated

(2906 F/g),[1] NiCo<sub>2</sub>S<sub>4</sub> nanosheets on N-modified carbon foam (1231 F/g),[17] Ni<sub>3</sub>S<sub>2</sub>@Ni(OH)<sub>2</sub> (1277 F/g),[9] NiCo<sub>2</sub>S<sub>4</sub> nanotubes (1093F/g),[7] Ni-Co-S nanowires (1176 F/g)[4] and Co<sub>9</sub>S<sub>8</sub> nanotube arrays (1775 F/g).[10] Although the electrode material is the key component that determines the capacitance value of electrode, the most definitive test for a new electrode material is how it performs in a full device.[18] More importantly, the charge-storage behavior of pseudocapacitive materials is strongly depending on the mass loading [19] and high capacitance can be obtained in practice only when the mass of active materials is at the level of less than one milligram per cm<sup>2</sup>. Therefore, pursuing high loading of active materials as well as high capacitance value are critical requirements for practical energy storage devices. However, simply increasing the mass-loading of conventional electrodes leads to an increase in “dead” materials, the part of which is not accessible to electrolyte and the utilization efficiency of active materials is low.[20] The design of hierarchical substrates for deposition of electroactive materials is highly desirable.

Here, we report the growth of VA-CNTs array on 3D CFP, which was further deposited with nickel-cobalt sulfide (Ni-Co-S) and polypyrrole (PPy). The 3D VA-CNTs/CFP is excellent substrate for the deposition of pseudoactive materials and allows for a large mass loading without mechanical peeling. The VA-CNTs array also provides effective electric transport between pseudoactive materials and the current collector, therefore, resulting in higher power density compared with randomly stacked CNTs. Due to the high surface area and well aligned structure, the Ni-Co-S and PPy are coated coaxially on individual CNT sidewall, which is believed to allow easy access of electrolyte for Faradiac reactions. More importantly, we describe for the first time the preparation of Ni-Co-S devices based on VA-CNTs/CFP substrate with high specific capacitance and excellent rate performance. A binder-free asymmetric energy storage (AES) devices with Ni-Co-S/VA-CNTs/CFP as the positive electrode and polypyrrole/VA-CNTs/CFP as the negative electrode respectively demonstrates high energy density of 82 Wh/kg at 200 W/kg. Two of such AES devices can power a LED light and toy fan.

## Results and discussion

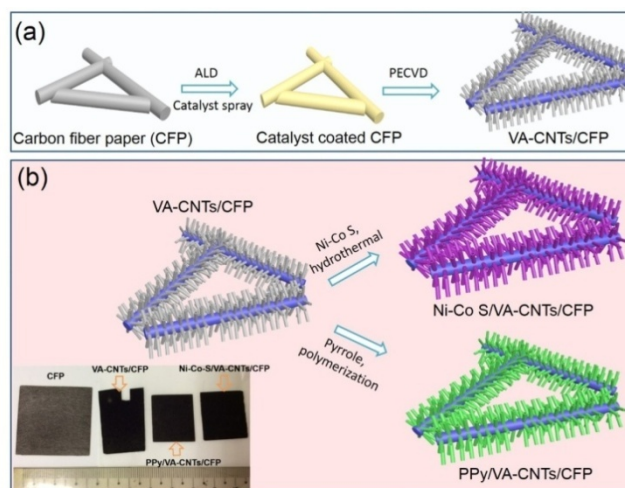


**Fig. 1** Schematic illustration of grown VA-CNTs on 3D CFP (a), and loading of pseudocapacitive materials Ni-Co-S and PPy (b). Inset (b) show the photograph of CFP, VA-CNTs/CFP, PPy/VA-CNTs/CFP, and Ni-Co-S/VA-CNTs/CFP samples.

Fig. 1 describes the procedure for the growth of VA-CNTs array on 3D CFP by PECVD method. Our group has previously reported the growth of VA-CNTs on cheap household Al foil for PEM fuel cell application.[21] Different from our previous work, a homogeneous thin layer of Al<sub>2</sub>O<sub>3</sub> with well-controlled thickness was first coated on plasma treated CFP by atomic layer deposition (ALD) method. The presence of homogeneous Al<sub>2</sub>O<sub>3</sub> coating is found essential to suppress the diffusion and aggregation of catalyst nanoparticles and thus leading to the formation of well-controlled VA-CNTs array. An ethanol solution containing Fe and Co acetate salts was evenly sprayed on CFP to synthesize FeCo bimetallic catalysts. After being calcined in air at 500°C for 5 min, the CFP coated with FeCo catalyst was placed into PECVD system. The growth of VA-CNT arrays were carried out at 700 °C for 30 min with ethylene as the carbon source. The Ni-Co-S nanoparticles were further grown on VA-CNTs backbone by hydrothermal method with thiourea as sulfur source. PPy was coated on VA-CNTs surface by chemical oxidation polymerization of pyrrole. The mass loading of Ni-Co-S and PPy on VA-CNTs/CFP was tuned by adjusting the concentration of the transition metal and monomer precursors. The size of the as-grown VA-CNTs/CFP samples are determined by the chamber volume of PECVD system. Large area of VA-CNTs/CFP can be produced for large AES devices. In this work, VA-CNTs/CFP with size over 100 cm<sup>2</sup> can be easily produced.

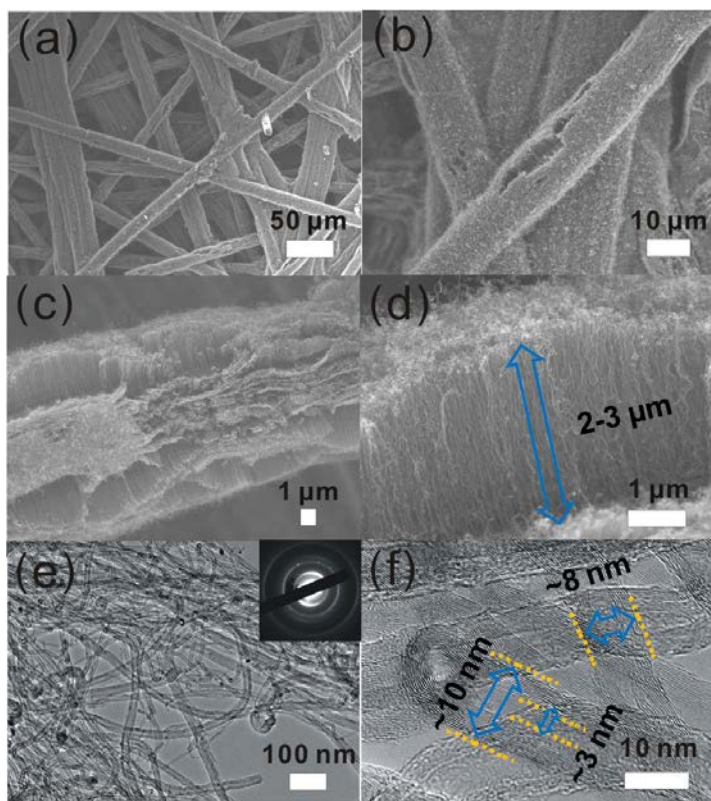


Fig. 2 SEM (a-d) and TEM (e-f) image of VA-CNT/CFP.

The SEM image of VA-CNTs/CFP is shown in Fig. 2. Pristine carbon fibers possess a very smooth surface with a diameter of  $\sim 7 \mu\text{m}$ . CNTs perpendicularly grown on the individual carbon fiber surface was observed with the average length of around 2-3  $\mu\text{m}$ , with outer and inner tube diameter of the CNT  $\sim 15$  and 3-7 nm, respectively. The presence of  $\text{Al}_2\text{O}_3$  buffer layer is essential. A control experiment was done, with all the other experimental procedure kept the same, but without the  $\text{Al}_2\text{O}_3$  coating layer. No VA-CNTs array was observed around CFP, indicating the crucial role of the  $\text{Al}_2\text{O}_3$  buffer layer (Fig. S1).

For an efficient CNTs growth, the catalyst-substrate interaction should be investigated with utmost attention, since the CNTs yield and structure strongly depends on the support materials.[4, 22] For example, with MgO as the support, Fe atoms can diffuse into MgO matrix at 500-800  $^\circ\text{C}$  by forming Fe-Mg-O alloy phase. The resultant Fe catalysts with smaller particle size are suitable for CNT growth.[4]  $\text{Al}_2\text{O}_3$  materials are better catalyst support than silica due to the strong metal-support interaction in the former,[6] which allows high catalyst dispersion and thus a high density of catalytic sites. Thin  $\text{Al}_2\text{O}_3$  flakes (0.04-4  $\mu\text{m}$  thick) loaded with iron nanoparticles have shown high yields of aligned CNTs of high aspect ratio.[5] In our PECVD method, a buffer layer of  $\text{Al}_2\text{O}_3$  is applied to separate the supporting substrate and catalyst nanoparticles. The direct coating of  $\text{Al}_2\text{O}_3$  homogeneously on substrate suppresses the diffusion and aggregation of catalyst nanoparticles, and promotes the aromatization of carbon atoms during CNT growth.[8] However, the presence of insulating  $\text{Al}_2\text{O}_3$  layer is unfavorable for energy storage applications; therefore, the thickness of the  $\text{Al}_2\text{O}_3$  layer was tuned from 1-5 nm to direct the growth of VA-CNTs. From Figs. S2a and b,

it can be seen that randomly oriented CNTs were grown on CFP with 1 nm thick  $\text{Al}_2\text{O}_3$  layer. This might be due to the reduction of catalytic sites by the diffusion of the catalyst nanoparticles within the substrate through uncoated area. A 3 nm thick  $\text{Al}_2\text{O}_3$  layer is sufficient to direct well-controlled growth of VA-CNTs on CFP (Figs 2, S1c and S1d). Further increase the thickness of the  $\text{Al}_2\text{O}_3$  layer to 5 nm does not lead to significant difference in the length and the density of the VA-CNTs (Figs S2e and f).

The mass loading of the catalyst ( $\text{mg}/\text{cm}^2$ ) was investigated to synthesize VA-CNTs/CFP with different inter-CNT distance. When the catalyst loading increases from 0.12 to 0.24 and then to 0.48  $\text{mg}/\text{cm}^2$  (Fig. S3), the VA-CNTs array turns from loosely-packed to densely packed, with inter-CNT distance decreases from  $\sim 50$  to 20 and then to 3-5 nm. At the low catalyst loading of 0.12  $\text{mg}/\text{cm}^2$ , the VA-CNTs with length of around 1  $\mu\text{m}$  cannot fully cover the carbon fiber, leaving plenty of exposed carbon fiber surface without CNTs. At the high catalyst loading of 0.48  $\text{mg}/\text{cm}^2$ , highly densely-packed VA-CNTs with numerous hemispheric prominences are observed on the surface of carbon fibers. Excessive catalyst loading leads to the generation of random and curl CNTs. Therefore, the optimum condition for the growth of VA-CNTs array on CFP is 3 nm thick  $\text{Al}_2\text{O}_3$  layer on plasma treated CFP at a FeCo catalyst loading of 0.24  $\text{mg}/\text{cm}^2$ . The presence of buffer layer was shown to be of significant importance to achieve perpendicularly oriented CNTs. The density of VA-CNTs is closely related to the mass loading of the catalyst, whilst the length of VA-CNTs is insensitive to buffer layer thickness. Unlike the growth of VA-CNTs on 2D smooth surface, such as Si and [23]graphene,[24] e-beam evaporation of Fe catalyst on  $\text{Al}_2\text{O}_3$  coated 3D substrate, such as Ni foam, does not produce VA-CNTs array under our experimental condition (Fig. S4).

The electrochemical performance of VA-CNTs/CFP was compared with CFP by measuring the cyclic voltammetry (CV) in KOH solution. The CV response of VA-CNTs/CFP reveals a significantly larger capacitive loop comparing to that of CFP, indicating a higher surface area and good electrical contact between VA-CNTs and carbon fibers. The CV measurement demonstrated that the VA-CNTs/CFP is highly capacitive. Further incorporation of pseudoactive materials will open up a wide range of potential applications (Fig. S5).

By using VA-CNTs/CFP as the substrate, we have prepared novel hybrid Ni-Co-S coaxial nanostructure on VA-CNTs/CFP (Ni-Co-S/VA-CNTs/CFP) by one-step hydrothermal process. The SEM and TEM images of Ni-Co-S/VA-CNTs/CFP are shown in Fig. 3. The advantage of this approach is the formation of triple components (Ni, Co and S) in one step without any post treatment. The SEM images illustrate the mesoporous structure of Ni-Co-S/VA-CNTs, which is composed of abundant Ni-Co-S sheets interconnecting with VA-CNTs. The VA-CNT array structure is well-kept. TEM images further reveal that the Ni-Co-S sheets intercross between CNTs with lateral size ranging from tens to hundred nanometers. The CNTs embedded between Ni-Co-S sheets can be clearly seen (Fig. 3b). High resolution TEM images further show the presence of ultra-small Ni-Co-S crystals with size of about 1-5 nm on the surface of CNTs (e and f). The lattice fringes of the Ni-Co-S crystals can be indexed to the 400 plane of  $\text{NiCo}_2\text{S}_4$ . In addition, the energy dispersive X-ray spectrometry (EDS) analysis was conducted to confirm the composition of Ni-Co-S/VA-CNTs/CFP. The elements, Cu (from TEM

grid), Ni, Co, S, and C were all detected. The EDS mapping clearly shows the homogeneous distribution of Ni, Co, S and C (Fig. S6), confirming the homogeneity of the composition and the uniform coating of Ni-Co-S on VA-CNTs surface.

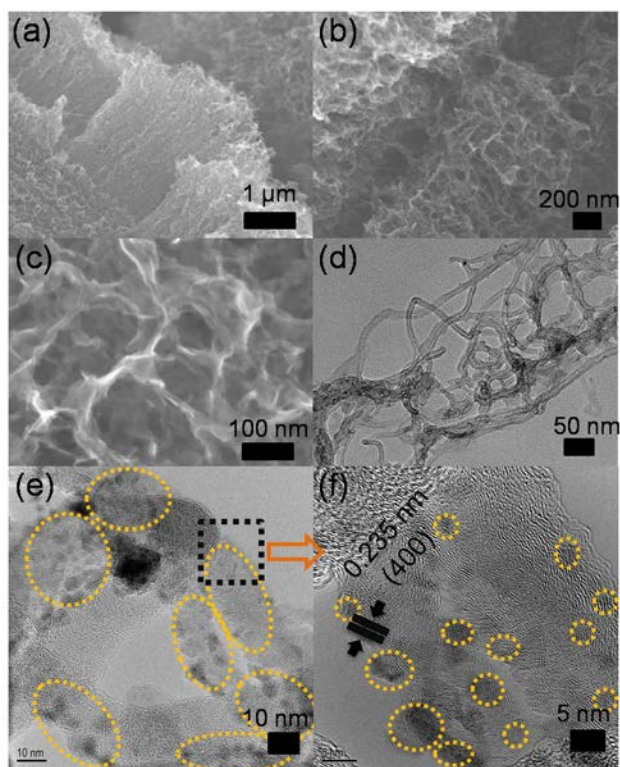


**Fig. 3** SEM images of Ni-Co-S/VA-CNTs/CFP (a-c) and TEM images of Ni-Co-S/VA-CNTs (d-e). HRTEM image from black dot square highlighted in (e) is shown in (f), where Ni-Co-S nanoparticles can be seen.

PPy was uniformly coated on VA-CNTs by chemical polymerization in an aqueous solution of 0.1M pyrrole. After coating of VA-CNTs by PPy, denser PPy/VA-CNT arrays with coarse surface are observed (Figs. 4a-d). The thickness of the PPy layer is identified from TEM images and is found to be in the range of around 3~10 nm (Figs. 4e and f). The SEM images of VA-CNTs/CFP before and after the deposition of PPy are shown in Fig. S6. The SEM images of PPy/VA-CNTs/CFP show that the CNTs have larger tube diameter with some areas conglutinated together, differing from that of the pristine VA-CNTs/CFP (Fig. S7). The TEM of individual PPy/VA-CNT show the PPy coating on CNT (small yellow arrow) which has a diameter of ~9.5 nm (large yellow arrow). The SEM and TEM measurement indicates that PPy formed a coaxial coating on the surface of individual CNT sidewall.

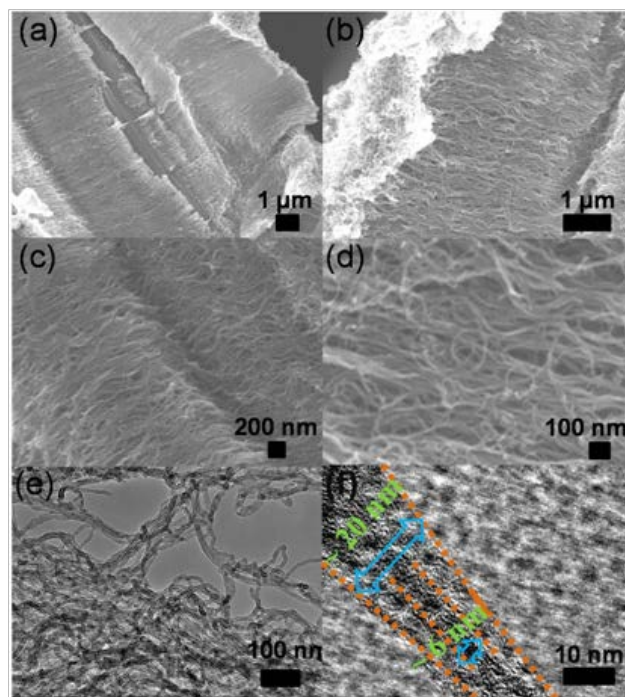


**Fig. 4** SEM (a-d) and TEM (e-f) images of PPy/VA-CNTs/CFP.

Raman spectroscopy was used to further characterize VA-CNTs/CFP and its composites. Typical G and D bands from CNTs are seen in Fig. 5. The Raman spectra of Ni-Co-S/VA-CNTs/CFP show negligible difference. For PPy/VA-CNTs/CFP, the peaks at 1050 and 1340  $\text{cm}^{-1}$  can be assigned to C-H in-plane deformation and C=C stretching of PPy, respectively. The peak at 986  $\text{cm}^{-1}$  is assigned to the ring deformation associated with radical cations.[25] The Raman study confirms the presence of PPy in PPy/VA-CNTs/CFP sample.

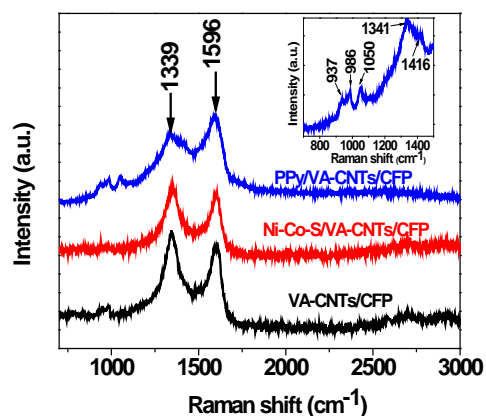


**Fig. 5** Raman spectra obtained for VA-CNTs/CFP, Ni-Co-S/VA-CNTs/CFP, and PPy/VA-CNTs/CFP

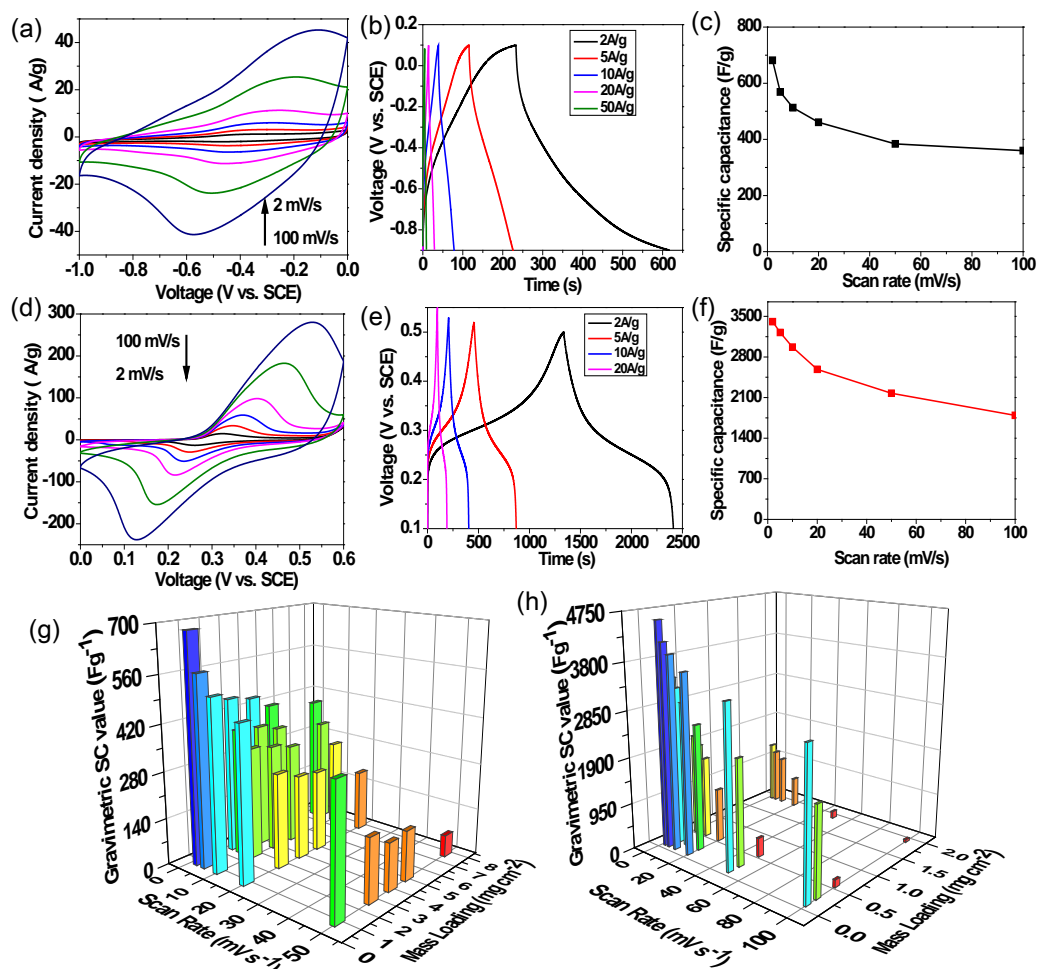


**Fig. 6** Electrochemical characterization of Ni-Co-S/VA-CNTs/CFP, and PPy/VA-CNTs/CFP electrodes. CV curves of PPy/VA-CNTs/CFP (a) and Ni-Co-S/VA-CNTs/CFP (d) at various scan rates from 2 to 100 mV/s. Charge discharge curves of PPy/VA-CNTs/CFP (b) and Ni-Co-S/VA-CNTs/CFP (e) at different current density from 2 to 50 and 200 A/g. Comparison of the specific capacitance as a function of current densities for PPy/VA-CNTs/CFP (c) and Ni-Co-S/VA-CNTs/CFP (f). The gravimetric specific capacitance values of PPy/VA-CNTs/CFP and Ni-Co-S/VA-CNTs/CFP with different mass loading of PPy and Ni-Co-S per  $\text{cm}^2$  as shown in (g) and (h) respectively.

Ni-Co-S and PPy are mainly coated on the sidewalls of VA-CNTs, forming vertically aligned integrated 3D structure. The VA-CNTs/CFP substrate serves as a high-surface-area scaffold for the deposition of Ni-Co-S and PPy. It also provides efficient transport channel for both electron and ions due to its high conductivity and highly aligned structure.

CV and galvanostatic charge-discharge measurements were performed to examine the potential of Ni-Co-S/VA-CNTs/CFP, and PPy/VA-CNTs/CFP as electrodes. The CV curves of PPy/VA-CNTs/CFP show obvious oxidation ( $-0.2\text{V}$ ) and reduction peaks ( $-0.6\text{V}$ ) of PPy at various scan rates from 2-100 mV/s. Fig. 6d shows the CV curves of Ni-Co-S/VA-CNTs/CFP in the 1 M KOH aqueous electrolyte with various sweeping rates ranging from 2-100 mV/s. A pair of redox

peaks is visible in all CV curves, revealing distinct pseudocapacitive characteristics, which are associated with the Faradaic redox reactions of transition metal sulfide.

The galvanostatic charge/discharge profiles of PPy/VA-CNTs/CFP and Ni-Co-S/VA-CNTs/CFP at different current densities are shown in Figs. 6b and e, respectively. A high specific capacitance (3407.9 F/g) was obtained at a scan rate of 2 mV/s, and the corresponding specific areal capacitance was  $0.86\text{ F/cm}^2$ . Even at a scan rate of 100 mV/s, the specific capacitance is still as high as 1792.2 F/g ( $0.45\text{ F/cm}^2$ ). It should be noted that the areal specific capacitance, regardless of the weight of sample, is a critical parameter for a practical electrode in energy storage devices. High areal specific capacitance requires not only high mass loading of the

electrochemically active materials per area, but also high utilization efficiency of the active materials.

The specific capacitance values of PPy/VA-CNTs/CFP calculated from CVs are 681, 568, 512, 480, and 384 F/g at scan rates of 2, 5, 10, 20 and 50 mV/s, respectively, corresponding to the areal capacitance of 0.78, 0.65, 0.58, 0.52 and 0.43 F/cm<sup>2</sup>. The mass loading of the active materials has significant effect on the gravimetric capacitance of the composite. The electrochemical behavior of VA-CNTs/CFP with different PPy and Ni-Co-S loadings were investigated. The gravimetric specific capacitance

decreases from 681 to 386 F/g when the loading of PPy increases from 0.84 to 7.75 mg/cm<sup>2</sup>, while the corresponding areal capacitance increases from 0.78 to 3.33 F/cm<sup>2</sup> when measured at a scan rate of 2 mV/s (Fig. 6g). The gravimetric specific capacitance of Ni-Co-S/VA-CNTs/CFP is 4569, 3407, 2100 and 1295 F/g when loading of Ni-Co-S increases from 0.09 to 0.25, 0.56 and then to 1.91 mg/cm<sup>2</sup>, while the corresponding areal capacitance increases from 0.41, to 0.85, 1.18, and 2.47 F/cm<sup>2</sup> (Fig. 6h).

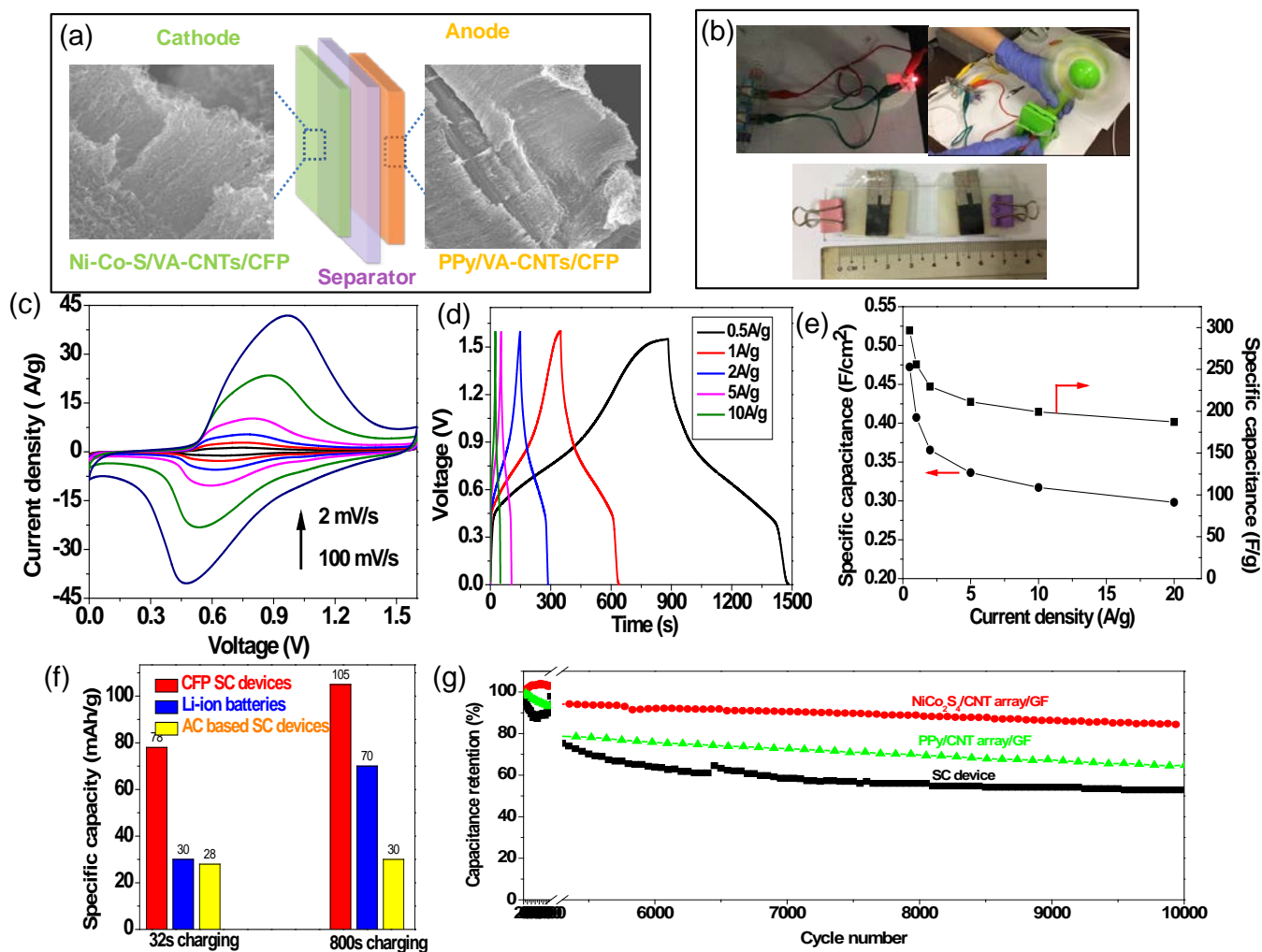


**Fig. 7** a) Schematic illustration of AES devices composed of Ni-Co-S/VA-CNTs/CFP as positive electrodes, and PPy/VA-CNTs/CFP as negative electrodes. b) Photograph of LED light and toy fan that are powered by the supercapacitor device as-shown below. c) CV curves of asymmetrical supercapacitor devices at various scan rates from 2 to 100 mV/s measured between 0-1.6V. d) Charge/discharge curves of asymmetrical supercapacitor devices at various current densities from 0.5 to 10 A/g, and the corresponding Specific areal and gravimetric capacitance (e). f) Comparison the specific capacities of ASC devices with commercial materials based Li-ion batteries (LiFePO<sub>4</sub>//graphite) and symmetrical supercapacitor (AC//AC). g) cycling stability of PPy/VA-CNTs/CFP, Ni-Co-S/VA-CNTs/CFP and as-assembled AES devices up to 10,000 cycles.

High areal specific capacitance value can be achieved with high mass loading of the active materials. However, this strategy is not practical for conventional 2D substrates, because higher loading may lead to cycling degradation and low charge storage efficiency.

The detachment of active materials from substrate and low conductivity caused by aggregation of semiconducting/insulating pseudocapacitive materials are the main reasons. Therefore, for practical applications, a balance between the utilization efficiency

of the active materials (low active materials loading) and areal specific capacitance (high mass loading active materials) has to be reached. Simply increase the loading of active materials on conventional substrate usually leads to an increase of “dead” materials, in which case, the electrolyte is inaccessible to the active materials. We show that our VA-CNTs/CFP having vertically aligned structure with well-controlled inter-CNT distance is an excellent substrate/scaffold for efficient loading and utilization of pseudocapacitive materials.

Asymmetric energy storage devices with Ni-Co-S/VA-CNTs/CFP as the positive electrode and PPy/VA-CNTs/CFP as the negative electrode in 1M KOH were fabricated. The mass loading of the two electrodes were balanced with the same areal capacitance before making the full cell devices. Fig. 7 shows the electrochemical performance of the ASC devices. A pair of distinct peaks is shown in CV curves under various scan rates, corresponding to the redox reactions of Ni-Co-S with alkaline electrolyte. The specific capacitance calculated from the charge and discharge curves shown in Fig. 7b are 296.6 F/g, 199.2 F/g and 187.2 at the current density of 0.5 A/g, 10 A/g, and 20A/g, respectively. The cell capacitance of the full device is calculated based on the total mass of the two electrodes, including CNTs and the active materials. Two ASC devices (each device has an area of 2 cm<sup>2</sup>) connecting in serial can power a LED light for more than ten minutes after being charged for 1~2 mins. A toy fan, which needs two AA batteries to power, can rotate robustly when powered by two ASC devices connecting in parallel.

The Nyquist plots show the charge-transfer resistance values are 0.85, 0.64, and 0.53 ohms for anode, cathode and ASC device, respectively. It is worthy to note that, the impedance analysis shows the ASC devices has battery type behavior. However, compared with conventional LiFePO<sub>4</sub> //graphite based Li-ion batteries, and activated carbon (AC) based symmetrical supercapacitors, the Ni-Co-S/VA-CNTs/CFP // PPy/VA-CNTs/CFP devices show significantly enhanced specific capacity value, at both high and low discharge current densities. At a charging time of 800 s, our ASC devices delivered specific capacity of 105 mAh/g, higher than Li-ion batteries (70 mAh/g) and AC based supercapacitors (30 mAh/g). At fast charging of 32s, the specific capacity of ASC device remains above 78 mAh/g, 2 times higher than that of Li-ion batteries.

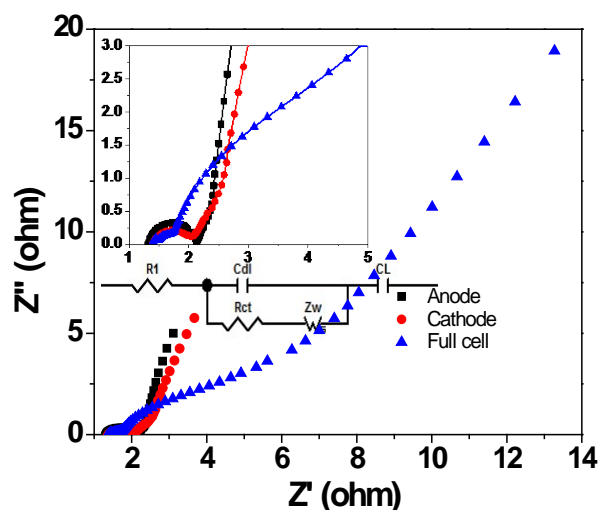


**Fig. 8** Nyquist impedance spectra of the anode, cathode electrodes, and ASC cell.

The cycling stability of the electrodes and the ASC device at a constant current density of 1 A/g is shown in Fig. 7h. The specific capacitance of Ni-Co-S/VA-CNTs/CFP is relatively stable with 84.4% capacity retention after 10,000 cycles. In order to match the areal capacitance of PPy/VA-CNTs/CFP with that of Ni-Co-S/VA-CNTs/CFP, the PPy loading is higher than 5 mg/cm<sup>2</sup>. The relatively high loading of PPy may be the main reason leading to the poor cyclability of the PPy/VA-CNTs/CFP (64.1% of capacity retention). As a result, the AES device maintained 52.8% of the capacity after 10,000 cycles. The laboratory assembly process may also contribute to the capacitance degradation with cycling. Nevertheless, the capacitance of the device after 10,000 cycles can still maintain above 100 F/g, significantly higher than AC based devices tested in our lab.

Ragone plot is shown in Fig. 9. The energy and power densities were calculated by following equations:

$$E = \frac{CV^2}{2 * 3.6} (Wh kg^{-1}) \quad eq. 1$$

$$P_{real} = \frac{E}{t} (W kg^{-1}) \quad eq. 2$$

Where  $C$  in F/g is the SC value of supercapacitor cell, the  $m$  is the total weight of electroactive materials at both electrodes. The assembled supercapacitor cells exhibit specific energy density of 82.4 and 52 Wh/kg when power density are 200 and 8000 W/kg, respectively. The Ni-Co-S/VA-CNTs/CFP//PPy/VA-CNTs/CFP cell outperforms some ASC devices in literature, such as Ni-Co-S nanowire// commercial activated carbon cell (25 Wh/kg at 3.57 kW/kg)[26], activated polyaniline derived carbon // Ni-Co oxide cell (41.6 Wh/kg at 16 kW/kg) [27], C/CoNi<sub>3</sub>O<sub>4</sub>//AC cell (19.2 Wh/kg at 13 kW/kg) [28], graphene-nickel cobaltite nanocomposite// activated carbon (7.6 wh/kg at 5.6 kW/kg) [29], Ni-Co oxide// activated carbon (7.4 Wh/kg at 1.9 kW/kg)[30], CoxNi<sub>1-x</sub>O/reduced G-O//reduced G-O cell (28 Wh/kg at 3614 W/kg),[31]Ni-Co hydroxides/Zn<sub>2</sub>SnO<sub>4</sub> // activated carbon devices (23.7 Wh/kg at 284 W/kg),[32]Ni-Co-S on carbon cloth//graphene films(60 Wh/kg at 1.8 kW/kg),[15]CoNi<sub>2</sub>S<sub>4</sub> nanosheet array on Ni foam // activated carbon device (33.9 Wh/kg at 409 W/kg)[33]. The energy density of 82.4 Wh/kg at 200 W/kg of our device is superior to aqueous and organic

electrolyte based EDLCs (3~15 Wh/kg). It also provides higher energy density than Li-ion batteries at the same power density.

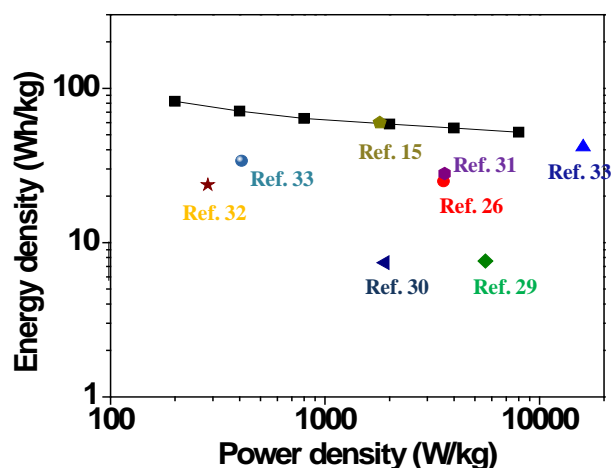


Fig. 9 Energy and power densities of our ASC devices compared with the data reported in other publications.

The specific areal capacitance values of the electrodes as a function of scan rates are shown in Fig. S8. The areal capacitance values of Ni-Co-S and PPy on carbon fiber paper are higher than most reported pseudocapacitive materials deposited on pure CFP substrate (Table S1). The areal capacitances of Ni-Co-S/VA-CNTs/CFP reach 2.5, 2.2, 1.9, 1.2 F/cm<sup>2</sup> when the specific gravimetric capacitance is 1294, 1146, 1016 and 633 F/g, respectively. The areal capacitance values of PPy/VA-CNTs/CFP are 3.3, 2.7, 2.2, 1.6 F/cm<sup>2</sup>, when the specific gravimetric capacitance values are 386, 319, 261, and 187 F/g, respectively. These results are remarkable compared to the early reported values for binder free electrodes and free-standing electrodes. The areal capacitances of Ni-Co-S and PPy on VA-CNTs/CFP substrate is higher than reported Co<sub>3</sub>O<sub>4</sub> on pristine CFP (0.95F/cm<sup>2</sup> at 5 mV/s).[18] Lou's group has grown NiCo<sub>2</sub>O<sub>4</sub> nanoneedles array on Ni foam surface, and high areal capacitance of 1.44 F/cm<sup>2</sup> was obtained at a discharge current of 2.78 mA/cm<sup>2</sup>. Fan's group designed a two-step hydrothermal method to synthesize hierarchical Co<sub>3</sub>O<sub>4</sub>@MnO<sub>2</sub> array on stainless steel substrate, and high areal capacitance of 0.56F/cm<sup>2</sup> was achieved at a discharge current of 11.25 mA/cm<sup>2</sup>.[20] Rational design of hierarchical substrate for deposition of electro active materials is one reasonable protocol to achieve high areal capacitance, such like CoNi<sub>2</sub>S<sub>4</sub> nanosheet array on Ni foam,[21] Co<sub>9</sub>S<sub>8</sub> nanotube array on Ni foam,[2] Ni-Co S nanowire on Ni foam,[3] cobalt sulfide nanosheets array on carbon cloth,[15] Ni<sub>3</sub>S<sub>2</sub> nanorod@Ni(OH)<sub>2</sub> nanosheet.[11] As shown in Fig. 10, low mass loading of electro active materials may not have strict requirement for substrate, only ultrathin coating of electro active materials on substrate can fully contribute the redox charge reversibly, due to the poor conductivity and mechanical properties of pseudocapacitive materials. The volume change during redox reaction of polymer and transition metal oxides causes low charge accumulation efficiency, where the redox reaction occurs mainly on or near surface rather than in the bulk. The crack of thick electro active materials coating on conventional electrodes further cause materials exfoliation, leading to capacitance degradation. The microstructure of VA-CNTs/CFP consists of vertically aligned CNTs

not only provide efficient transport channel for electrons and ions, but also provide backbone for ultrathin, high efficient deposition of electro active materials, both ensures high mass loading and high areal capacitance of electrodes.

The good performance of our ASC device can be ascribed to the following features of the electrodes: 1) well-aligned CNTs provide electric channel for efficient transportation of charges; 2) VA-CNTs with high surface area is excellent scaffold for the incorporation of pseudocapacitive materials; 3) 3D CFP composed of interconnected carbon fibers (8 μm diameter) not only provides sufficient space for the growth of VA-CNTs, it also serves as a strong mechanical support; 4) coaxial deposition of thin layer of pseudoactive materials on side-wall of CNTs ensures efficient charge transfer, shortens the diffusion length and improves the utilization efficiency of the pseudoactive materials.

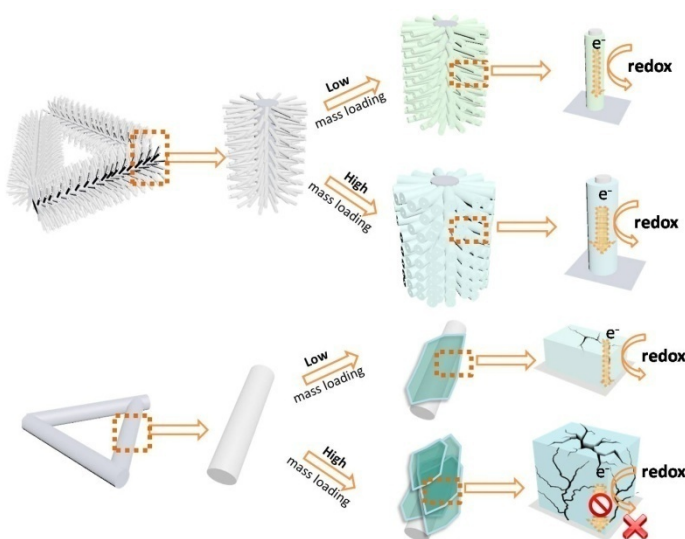


Fig. 10 Comparison of conventional 2D or 3D CFP and hierarchical 3D VA-CNTs/CFP based substrate when used for deposition of active materials.

## Conclusions

In summary, we designed a PECVD method for the growth of VA-CNTs on porous 3D CFP substrate. The catalyst preparation is the key step for the growth of well-controlled VA-CNTs. The effect of Al<sub>2</sub>O<sub>3</sub> buffer layer and the catalyst loading on the structure of VA-CNTs have been investigated. The rational design and growth of Ni-Co-S and PPy on VA-CNTs/CFP is presented, and is demonstrated as a novel freestanding electrode for energy storage applications. The gravimetric specific capacitance of the electrodes depends on the mass loading of the pseudocapacitive materials (Ni-Co-S and PPy). The specific capacitance of Ni-Co-S/VA-CNTs/CFP (4569F/g) decreased by 4 times (1268 F/g) when the mass loading of Ni-Co-S increased from 0.09 to 1.91 mg/cm<sup>2</sup>. A binder-free asymmetric energy storage device is fabricated by using Ni-Co-S/VA-CNTs/CFP as the positive electrode and PPy/VA-CNTs/CFP as the negative electrode, respectively. The device delivers high energy density of 82 Wh/kg at 200 W/kg. The synthesis of VA-CNTs can be easily scaled up. A variety of other 3D based substrates, besides the

commercially available CFP that we have demonstrated here, can be used for the growth of VA-CNTs. We believe our findings will enable the preparation of advanced energy storage electrodes promising for portable electronics, wearable energy storage devices and many other applications.

## Experimental

### Materials

The carbon fiber paper used was Toray Carbon Paper 060. Pyrrole was purchased from Sigma-Aldrich and distilled under reduced pressure before use. All gases were supplied by Soxal Pte. Ltd. All other chemicals were purchased from Alfa Aesar and used as-received.

### Fabrication of VA-CNTs/CFP

The vertically aligned CNT (VACNT) on carbon fiber paper substrate was fabricated using a PECVD approach similar to the method reported by Tian et al.[34]. Basically, a piece of carbon fiber paper with the dimension of 5.5 cm × 4cm was treated with oxygen plasma with a power of 80W for 90s and coated with 3nm of Al<sub>2</sub>O<sub>3</sub> using atomic layer deposition. The carbon fiber paper was then fixed on a hotplate set at 90 °C. 4 ml of 7mM iron acetate and 7mM cobalt acetate ethanol solution were evenly sprayed on each side of the carbon fiber paper. Heat treatment was carried out at 500 °C for 10 min in air to synthesize Fe-Co bimetallic catalyst.

The carbon fiber paper was put in the chamber of plasma-enhanced chemical vapor deposition (PECVD) system. The sample chamber was first evacuated to a pressure of 10<sup>-5</sup> Pa, then 20 sccm of H<sub>2</sub> gas was supplied into the chamber. The pressure was then maintained at 133Pa. The temperature inside the chamber was ramped from room temperature to 700°C at a rate of 100°C min<sup>-1</sup>. Once the temperature reached 700 °C, the a radio frequency alternating magnetic field with a power of 30 W was switch on to treat the FeCo bimetallic catalyst using hydrogen plasma for 2 min. Then the 20 sccm flow rate of H<sub>2</sub> flow was maintained and 40 sccm of C<sub>2</sub>H<sub>2</sub> was introduced into the chamber. The air flow was kept for 20 min to grow VACNTs. Finally the chamber was cooled down to room temperature.

### Synthesis of PPy/VA-CNTs/CFP

PPy/VA-CNTs/CFP was synthesized by oxidative polymerization similar to our previous works.[35, 36] The substrate was cut to a 5.5 cm × 2cm dimension. It was then treated with oxygen plasma with a power of 80W for 30s to increase the wettability of the VACNTs. The substrate was then weighted and put in a beaker containing 100ml of 0.1mol L<sup>-1</sup>HCl and 0.1mmol (6.9μl) of Pyrrole. The beaker was then put into ice bath and magnetically stirred for 10 mins to allow the substrate to fully absorb the solution. 3 ml of 0.1mol L<sup>-1</sup> FeCl<sub>3</sub> and 0.1mol L<sup>-1</sup> LiClO<sub>4</sub> solution was added drop by drop into the mixture. The reaction was then kept for 8 hrs. The product was then washed by ethanol and DI water, and dried at 60 °C under vacuum.

### Synthesis of Ni-Co-S /VA-CNTs/CFP

Ni-Co-S/VA-CNTs/CFP was synthesized using a simple one-step hydrothermal method. The substrate was cut and treated with oxygen plasma as described in the previous section. 100ml of

solution containing 1mmol L<sup>-1</sup> NiNO<sub>3</sub>, 1mmol L<sup>-1</sup> CoNO<sub>3</sub> and 0.2mol L<sup>-1</sup> thiourea was put into a sealable glass container. Diluted NH<sub>3</sub>·H<sub>2</sub>O was added into the solution to adjust the pH value so that the pH was around 8 and the color of the solution was a light blue. The substrate was then put into the container. The reaction container was then put into an oil bath pre-heated to 95°C. The reaction was then carried out under magnetic stirring for 8 hrs. The product was then washed by DI water and dried.

### Characterizations and Electrochemical Testing

The samples were examined using a JEOL JSM-6700F scanning electron microscope (SEM) and high resolution JEOL 2100 transmission electron microscope (TEM). Electrochemical measurements were carried out using 1M KOH as electrolyte on CHI-760d electrochemical workstation. The electrochemical impedance spectroscopy (EIS), cyclic voltammetry (CV) and galvanostatic charge/discharge measurements were obtained in both 3-electrodesystem with SCE as the reference electrode and 2-electrode system respectively. Cycle life tests were also carried out for anode material and cathode material in 3-electrode system and full cell in 2-electrode system for over 10000 cycles.

The capacitance can be calculated from the CV curves according to the equation:

$$C = \frac{(\int idV)}{v\Delta V} \quad \text{eq. 3}$$

The specific capacitance calculated using equation:

$$C = \frac{i \times \Delta t}{m \times \Delta V} \quad \text{eq. 4}$$

where  $i$  is the discharge current,  $\Delta t$  is the discharge time,  $v$  is the scan rate (mV s<sup>-1</sup>),  $m$  is the mass of the active material (weight of Ni-Co-S or PPy + VA-CNTs), and  $\Delta V$  is the potential window.

To assembly asymmetric supercapacitor, the areal capacity of cathode and anode are balanced:

$$C_{\text{areal}} = \frac{(\int idV)}{vAV} \quad \text{eq. 5}$$

where  $A$  is the geometric area of electrode. The loading mass of Ni-Co-S and PPy were tuned, until the  $C_{\text{areal}}$  of cathode and anode is equal.

### Acknowledgements

The authors gratefully acknowledge Mr Chao Dongliang and Ms Wang Jin for useful discussions.

### References

- 1 T. W. Ebbesen and P. M. Ajayan, *Nature*, 1992, **358**, 220-222.
- 2 J. Pu, Z. H. Wang, K. L. Wu, N. Yu and E. H. Sheng, *Phys. Chem. Chem. Phys.*, 2014, **16**, 785-791.
- 3 Y. H. Li, L. J. Cao, L. Qiao, M. Zhou, Y. Yang, P. Xiao and Y. H. Zhang, *J. Mater. Chem. A*, 2014, **2**, 6540-6548.
- 4 H. Ago, K. Nakamura, N. Uehara and M. Tsuji, *J. Phys. Chem. B*, 2004, **108**, 18908-18915.
- 5 C. L. Pint, S. T. Pheasant, M. Pasquali, K. E. Coulter, H. K. Schmidt and R. H. Hauge, *Nano. Lett.*, 2008, **8**, 1879-1883.
- 6 N. Nagaraju, A. Fonseca, Z. Konya and J. B. Nagy, *J. Mol. Catal. a-Chem.*, 2002, **181**, 57-62.
- 7 L. T. Qu, Y. Zhao and L. M. Dai, *Small*, 2006, **2**, 1052-1059.

- 8 A. J. Hart, A. H. Slocum and L. Royer, *Carbon*, 2006, **44**, 348-359.
- 9 E. T. Thostenson, W. Z. Li, D. Z. Wang, Z. F. Ren and T. W. Chou, *J. Appl. Phys.*, 2002, **91**, 6034-6037.
- 10 F. Du, D. S. Yu, L. M. Dai, S. Ganguli, V. Varshney and A. K. Roy, *Chem. Mater.*, 2011, **23**, 4810-4816.
- 11 W. J. Zhou, X. H. Cao, Z. Y. Zeng, W. H. Shi, Y. Y. Zhu, Q. Y. Yan, H. Liu, J. Y. Wang and H. Zhang, *Energ. Environ. Sci.*, 2013, **6**, 2216-2221.
- 12 A. S. Arico, P. Bruce, B. Scrosati, J. M. Tarascon and W. Van Schalkwijk, *Nat. Mater.*, 2005, **4**, 366-377.
- 13 J. Xu, Q. F. Wang, X. W. Wang, Q. Y. Xiang, B. Hang, D. Chen and G. Z. Shen, *Acs Nano*, 2013, **7**, 5453-5462.
- 14 X. H. Xia, C. R. Zhu, J. S. Luo, Z. Y. Zeng, C. Guan, C. F. Ng, H. Zhang and H. J. Fan, *Small*, 2014, **10**, 766-773.
- 15 W. Chen, C. Xia and H. N. Alshareef, *ACS Nano*, 2014, **8**, 9531-9541.
- 16 G. A. Snook, P. Kao and A. S. Best, *J. Power Sources*, 2011, **196**, 1-12.
- 17 L. F. Shen, J. Wang, G. Y. Xu, H. S. Li, H. Dou and X. G. Zhang, *Adv. Energy. Mater.*, 2015, **5**, 1400977-1400985.
- 18 J. H. Kwak, Y. W. Lee and J. H. Bang, *Mater. Lett.*, 2013, **110**, 237-240.
- 19 L. B. Hu, W. Chen, X. Xie, N. A. Liu, Y. Yang, H. Wu, Y. Yao, M. Pasta, H. N. Alshareef and Y. Cui, *Acs Nano*, 2011, **5**, 8904-8913.
- 20 J. P. Liu, J. Jiang, C. W. Cheng, H. X. Li, J. X. Zhang, H. Gong and H. J. Fan, *Adv. Mater.*, 2011, **23**, 2076-2081.
- 21 W. Hu, R. Q. Chen, W. Xie, L. L. Zou, N. Qin and D. H. Bao, *Acs Appl. Mater. Inter.*, 2014, **6**, 19318-19326.
- 22 M. Kumar and Y. Ando, *J. Nanosci. Nanotechnol.*, 2010, **10**, 3739-3758.
- 23 A. J. Hart and A. H. Slocum, *J. Phys. Chem. B*, 2006, **110**, 8250-8257.
- 24 R. K. Paul, M. Ghazinejad, M. Penchev, J. A. Lin, M. Ozkan and C. S. Ozkan, *Small*, 2010, **6**, 2309-2313.
- 25 V. Varade, G. V. Honnavar, P. Anjaneyulu, K. P. Ramesh and R. Menon, *J. Phys. D: Appl. Phys.*, 2013, **46**, 365306.
- 26 Y. Li, L. Cao, L. Qiao, M. Zhou, Y. Yang, P. Xiao and Y. Zhang, *J. Mater. Chem. A*, 2014, **2**, 6540-6548.
- 27 R. Wang and X. Yan, *Sci. Rep.*, 2014, **4**, 3712-3721.
- 28 J. Zhu, J. Jiang, Z. Sun, J. Luo, Z. Fan, X. Huang, H. Zhang and T. Yu, *Small*, 2014, **10**, 2937-2945.
- 29 H. Wang, C. B. Holt, Z. Li, X. Tan, B. Amirkhiz, Z. Xu, B. Olsen, T. Stephenson and D. Mitlin, *Nano Res.*, 2012, **5**, 605-617.
- 30 C. Tang, Z. Tang and H. Gong, *J. Electrochem. Soc.*, 2012, **159**, A651-A656.
- 31 J. Xiao and S. Yang, *J. Mater. Chem.*, 2012, **22**, 12253-12262.
- 32 X. Wang, A. Sumboja, M. Lin, J. Yan and P. S. Lee, *Nanoscale*, 2012, **4**, 7266-7272.
- 33 W. Hu, R. Chen, W. Xie, L. Zou, N. Qin and D. Bao, *ACS Appl. Mater. Inter.*, 2014, **6**, 19318-19326.
- 34 Z. Q. Tian, S. H. Lim, C. K. Poh, Z. Tang, Z. Xia, Z. Luo, P. K. Shen, D. Chua, Y. P. Feng, Z. Shen and J. Lin, *Adv. Energy Mater.*, 2011, **1**, 1205-1214.
- 35 L. F. Lai, L. Wang, H. P. Yang, N. G. Sahoo, Q. X. Tam, J. L. Liu, C. K. Poh, S. H. Lim, Z. X. Shen and J. Y. Lin, *Nano Energy*, 2012, **1**, 723-731.
- 36 X. Cai, S. H. Lim, C. K. Poh, L. Lai, J. Lin and Z. Shen, *J. Power Sources* 2015, **275**, 298-304.